MEDWIN PUBLISHERS
Committed to create value for Researchers

Nanomedicine & Nanotechnology Open Access
ISSN: 2574-187X

# Spectroscopic Characterization, Quantum Computational and Molecular Docking Studies on 3-Isopropoxy-2-Naphthoic Acid: A Potential Antibacterial Agent

**Vetrivelan V[1]* and Sathyaseelan B[2]**

[1]Department of Physics, Thanthai Periyar Government Institute of Technology, India

[2]Department of Physics, University college of Engineering Arni, India

***Corresponding author**: Vetrivelan V, Department of Physics, Thanthai Periyar Government Institute of Technology, Vellore 632 002, Tamilnadu, India, Tel: +91-9486898120; Email: vetri.tpgit@gmail.com

**Research Article**

Volume 3 Issue 3

**Received Date**: August 06, 2018

**Published Date:** September 10, 2018

**DOI:** 10.23880/nnoa-16000148

## Abstract

In the present study, Quantum chemical approach was carried out on the title compound 3-isopropoxy-2-naphthoic acid (3IP2NA) to study the vibrational spectrum, the stability of the compound, the intramolecular and intermolecular interactions using DFT with B3LYP/6-311++G (d,p) basis set. The observed FT-IR and FT-Raman spectra were recorded in the region 4000–450 $cm^{-1}$ and 4000-100 $cm^{-1}$ and compared with computational data. The vibrational assignments of wave numbers were made on the basis of PED by VEDA 4 programme. The optimized molecular geometry, vibrational wave numbers, infrared intensities and Raman scattering activities were calculated. Several descriptors determined from the energies of frontier molecular orbital were applied to describe the reactivity of the 3IP2NA. The electron density based local reactivity descriptors such as Fukui functions were calculated to explain the chemical selectivity or the reactivity site in the 3IP2NA. The thermodynamic properties of the 3IP2NA were determined at different temperatures. Molecular docking studies were made on 3IP2NA to study the hydrogen bond interactions and the minimum binding energy was calculated.

**Keywords:** FT-IR; FT-Raman; DFT; NBO; Fukui Function; Molecular Docking

**Abbreviations:** PED: Potential Energy Distribution; ED: Electron Density; NBO: Natural Bond Orbital; FMOs: Frontier Molecular Orbital's; MEP: Molecular Electrostatic Potential; NLO: non-linear optical; ICT: intermolecular charge transfer; IP: ionization potential.

## Introduction

The new molecular manipulation approach leads to the development of new drugs. As a result, the antimicrobial studies are the best way to overcome

microbial resistance and to develop effective therapies. Despite of enormous progress in medicinal chemistry, communicable diseases continue a major threat to our society and have provided a new challenge to researcher's worldwide [1]. The new molecular manipulation directs to approach the development of new drugs [2,3]. Among various diseases, malaria and microbial infections are the widest spreading in nature [4-6]. As a result, the antimicrobial studies are the best way to overcome microbial resistance and to develop effective therapies [7]. Our title compound 3IP2NA have exhibit interesting biological activities such as Sphingosine kinase inhibitor, Chymosin inhibitor, beta-adrenergic receptor kinase inhibitor, G-protein-coupled receptor kinase inhibitor, Phobic disorders treatment etc.

Even though a lot of experimental studies available, but there is a no evidence for theoretical studies of the 3IP2NA compound. Hence, an attempt has been made to present work to analyze IP2NA compound theoretically and these results are supported by experimental FT-IR and FT-Raman Spectral data.

A systematic study of the molecule detailed design and vibrational spectra aid in understanding the property of the 3IP2NA in-depth insight. Vibrational spectra of the title compound have been analyzed on the basis of Potential Energy Distribution (PED). The modification in Electron Density (ED) in the σ* and π* anti bonding orbital's and stabilization energies E(2) has been calculated by Natural Bond Orbital (NBO) investigation to give clear evidence of stabilization originating in the hyper conjugation of hydrogen–bond interaction. Frontier Molecular Orbital's (FMOs) and Thermodynamic properties of the title compound at various temperatures were calculated. Molecular Electrostatic Potential (MEP) and non-linear optical (NLO) properties of the 3IP2NA at DFT (B3LYP) with the 6-311++G (d,p) level. The molecular docking can predict the binding energy of the ligand with respect to the protein 4XUV and 4M1C to form a stable complex.

## Material and Methods

### Experimental Details

The 3IP2NA compound in the solid state was procured from Sigma–Aldrich chemical company with a stated purity 98% and it was used without further purification. The FT-IR spectrum was recorded in the region 4000–450 $cm^{-1}$ with the sample in the KBr pellet, using Perkin Elmer FT-IR spectrometer. The resolution of the spectrum is 4 $cm^{-1}$. The FT-Raman spectrum was obtained in the range 4000–100 $cm^{-1}$ using Bruker RFS 100/S FT-Raman spectrophotometer with a 1064 nm Nd: YAG laser source of 100 mW power.

### Computational Details

Entire theoretical calculations of 3F4PBA were work out by DFT/B3LYP method with 6-311++G (d, p) basis set using Gaussian 09 software package [8]. Gauss view molecular visualization program [9] is used to visualize the geometry structure. The theoretical vibrational assignments were interpreted by means of PED (Potential Energy Distribution) using VEDA 4 program [10]. Molecular docking studies give vital details about orientation of 3IP2NA (ligands) which regulate the binding affinity between the ligand and their protein target. Molecular docking studies were carried out using Auto Dock 4.2 software [11].

### Prediction of Raman Intensities

The calculated Raman activities ($S_i$) converted to relative Raman intensities ($I_i$) using the following relations [12].

$$I_i = \frac{f(\upsilon_0-\upsilon_i)^4 S_i}{\upsilon_i [1 - \exp (hc\upsilon i/k_b T)]},$$

Where, $\upsilon_0$ is the exciting frequency in $cm^{-1}$ $\upsilon_i$ is the vibrating wave number of the $i^{th}$ normal mode *h*, c and $k_b$ are the fundamental constants and f is a normalization factor for all peak intensities.

## Results and Discussion

### Geometrical Structure

The optimized structure parameters of the 3IP2NAwere calculated at B3LYP levels and are recorded in Table 1 in accordance with the atom numbering scheme as obtained from CHEMCRAFT software and represented in (Figure 1). This molecule has fourteen C-C bond lengths, three C-O bond lengths, thirteen C-H bond lengths, one C=O bond lengths and one O-H bond length. The molecular geometry in the gas phase may differ from the solid phase owing to the extended hydrogen bonding and staking interactions. From theoretical values, any variation in the optimized bond lengths is because the theoretical values belong to the isolated molecules in the gas phase and the experimental values belong to the molecules in solid state [13]. It is observed that the

calculated C-C bond lengths and the O-C bond lengths are found to be nearly identical at all calculation levels. The average value of the bond distances of C-C and C-H in the benzene ring calculated by DFT method with same basis sets are 1.4535 A and 1.088 A, respectively. The inclusion of O-H and C-H atoms brings a strong electron-withdrawing nature to the compound and thus is expected to contribute to the formation of a resonance structure. This is the reason for the shortening of bond lengths O13-H24 = 0.968 Å and C9-H23 = 1.085 Å obtained by DFT method compared to other bond lengths like C2-C11 = 1.489 Å. In this title molecule the bond angle C11-O13-H24= 106° is smaller than the other bond angle C4-C3-O14 = 124.8° calculated.

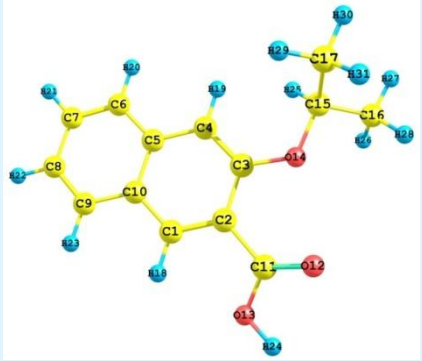


Figure 1: Optimized geometric structure with atom numbering of 3IP2NA.

| Atoms | DFT | Atoms | DFT | Atoms | DFT |
|---|---|---|---|---|---|
| Bond Length (Å) | | Bond Angle ( 0 ) | | Bond Angle ( 0 ) | |
| C1-C2 | 1.38 | C2-C1-C10 | 122.2 | C10-C9-H23 | 118.8 |
| C1-C10 | 1.414 | C2-C1-H18 | 118.8 | O12-C11-O13 | 121.2 |
| C1-H18 | 1.083 | C1-C2-C3 | 119.4 | C11-O13-H24 | 106 |
| C2-C3 | 1.438 | C1-C2-C11 | 119.2 | O14-C15-C16 | 105.4 |
| C2-C11 | 1.489 | C10-C1-H18 | 119 | O14-C15-C17 | 110.4 |
| C3-C4 | 1.381 | C1-C10-C5 | 118.2 | O14-C15-H25 | 108.7 |
| C3-O14 | 1.35 | C1-C10-C9 | 122.3 | C16-C15-C17 | 112.7 |
| C4-C5 | 1.418 | C3-C2-C11 | 121.4 | C16-C15-H25 | 109 |
| C4-H19 | 1.081 | C2-C3-C4 | 119.3 | C15-C16-H26 | 110.6 |
| C4-C6 | 1.42 | C2-C3-O14 | 115.8 | C15-C16-H27 | 110.2 |
| C5-C10 | 1.428 | C2-C11-O12 | 127 | C15-C16-H28 | 110.3 |
| C6-C7 | 1.375 | C2-C11-O13 | 111.7 | C17-C15-H25 | 110.4 |
| C6-H20 | 1.085 | C4-C3-O14 | 124.8 | C15-C17-H29 | 111.9 |
| C7-C8 | 1.415 | C3-C4-C5 | 121.5 | C15-C17-H30 | 110.1 |
| C7-H21 | 1.084 | C3-C4-H19 | 120.5 | C15-C17-H31 | 109.9 |
| C8-C9 | 1.374 | C3-O14-C15 | 121.6 | H26-C16-H27 | 108.6 |
| C8-H22 | 1.084 | C5-C4-H19 | 117.9 | H26-C16-H28 | 108.4 |
| C9-C10 | 1.419 | C4-C5-C6 | 122.2 | H27-C16-H28 | 108.7 |
| C9-H23 | 1.085 | C4-C5-C10 | 119.3 | H29-C17-H30 | 108.1 |
| C11-O12 | 1.206 | C6-C5-C10 | 118.5 | H29-C17-H31 | 108.3 |
| C11-O13 | 1.367 | C5-C6-C7 | 120.7 | H30-C17-H31 | 108.5 |
| O13-H24 | 0.968 | C5-C6-H20 | 119 | | |
| O14-C15 | 1.445 | C5-C10-C9 | 119.5 | | |
| C15-C16 | 1.522 | C7-C6-H20 | 120.3 | | |
| C15-C17 | 1.527 | C6-C7-C8 | 120.7 | | |
| C15-H25 | 1.096 | C6-C7-H21 | 119.8 | | |
| C16-H26 | 1.092 | C8-C7-H21 | 119.5 | | |
| C16-H27 | 1.093 | C7-C8-C9 | 119.9 | | |
| C16-H28 | 1.092 | C7-C8-H22 | 119.8 | | |
| C17-H29 | 1.092 | C9-C8-H22 | 120.3 | | |
| C17-H30 | 1.094 | C8-C9-C10 | 120.7 | | |
| C17-H31 | 1.093 | C8-C9-H23 | 120.5 | | |

Table 1: Optimized geometrical parameters of 3IP2NA.

## Vibrational Spectral Analysis

Experimental and theoretical comparative FT-IR and FT-Raman spectra of 3IP2NA molecule are shown in (Figures 2a & b). The 3IP2NA molecule consists of 31 atoms, therefore, they have 87modes of vibration since it is nonlinear structure. The Vibrational frequencies are scaled 0.961 [14] for B3LYP/6-311++G (d,p) in order to compensate for the errors arising from the basis set incompleteness and neglect the vibrational an harmonicity. The measured (FT-IR and FT-Raman) wave numbers and assigned wave numbers values are given in Table 2. This reveals good correspondence between theory and experiment in main spectral features.

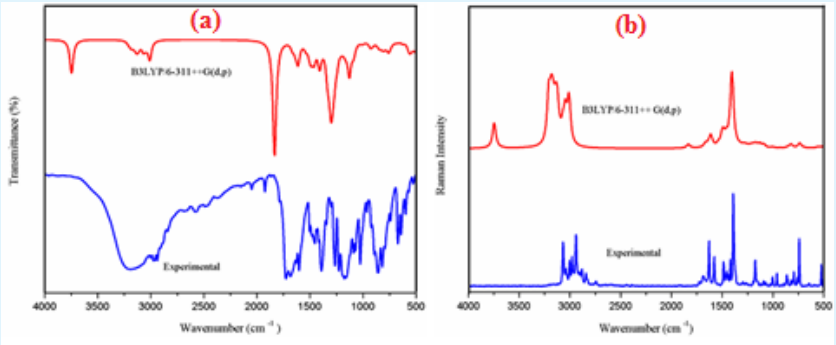


Figure 2: (a) Comparative FT-IR spectra and (b) Comparative Raman spectra of 3IP2NA.

| Mode No. | Wave number ($cm^{-1}$) | | | | Intensity | | | | Assignments (PED≥10%)d |
|---|---|---|---|---|---|---|---|---|---|
| | Experimental | | Theoretical | | FT-IR | | Raman | | |
| | FT-IR | Raman | Un- scaled | Scaled[a] | Relative[b] | Absolute | Relative[b] | Absolute | |
| 87 | - | - | 3746 | 3611 | 129 | 29 | 141 | 42 | υOH(100) |
| 86 | - | - | 3209 | 3094 | 5 | 1 | 202 | 60 | υCH (90) |
| 85 | - | - | 3209 | 3093 | 6 | 1 | 46 | 14 | υCH (89) |
| 84 | 3190 | 3067 | 3184 | 3070 | 20 | 4 | 177 | 53 | υCH (53) |
| 83 | - | - | 3169 | 3055 | 4 | 1 | 70 | 21 | υCH (95) |
| 82 | - | - | 3167 | 3053 | 2 | 0 | 61 | 18 | υCH (96) |
| 81 | - | 3042 | 3151 | 3038 | 10 | 2 | 62 | 19 | υCH (98) |
| 80 | - | - | 3138 | 3025 | 18 | 4 | 109 | 33 | υCH (90) |
| 79 | - | - | 3125 | 3013 | 17 | 4 | 142 | 43 | υCH (73) |
| 78 | 3000 | 3004 | 3112 | 3000 | 16 | 4 | 35 | 10 | υCH (97) |
| 77 | 2973 | 2978 | 3070 | 2960 | 33 | 7 | 70 | 21 | υCH (50) |
| 76 | 2938 | 2940 | 3046 | 2936 | 17 | 4 | 161 | 48 | υCH (58) |
| 75 | - | 2908 | 3010 | 2901 | 6 | 1 | 88 | 26 | υCH (87) |
| 74 | 2841 | 2882 | 3009 | 2901 | 65 | 15 | 161 | 48 | υCH (93) |
| 73 | 1786 | 1726 | 1834 | 1768 | 442 | 100 | 21 | 6 | υOC (94) |
| 72 | 1603 | 1629 | 1665 | 1605 | 22 | 5 | 21 | 6 | υOC (62)+υCC (34) |
| 71 | - | 1579 | 1636 | 1577 | 26 | 6 | 10 | 3 | υCC (55) |
| 70 | 1503 | - | 1612 | 1554 | 76 | 17 | 64 | 19 | υCC (26)+βCCC (14) |
| 69 | 1481 | 1487 | 1538 | 1483 | 20 | 4 | 14 | 4 | υCC (28)+βHCC (13) |
| 68 | 1454 | 1455 | 1505 | 1451 | 23 | 5 | 5 | 2 | βHCH (60) |
| 67 | - | 1438 | 1499 | 1445 | 3 | 1 | 36 | 11 | βHCH (15) |
| 66 | - | - | 1495 | 1442 | 4 | 1 | 15 | 4 | βHCH (70)+τHCCC (11) |
| 65 | - | - | 1492 | 1439 | 9 | 2 | 15 | 5 | βHCH (34)+τHCOC (14) |
| 64 | 1435 | - | 1491 | 1437 | 23 | 5 | 5 | 2 | βHCC (11)+βHCH (43) |

| | | | | | | | | | |
|---|---|---|---|---|---|---|---|---|---|
| 63 | - | 1419 | 1482 | 1429 | 16 | 4 | 12 | 4 | β HCH (53) |
| 62 | 141 | 1391 | 1461 | 1408 | 57 | 13 | 42 | 13 | υCC (20)+βHCC (28) |
| 61 | 1393 | - | 1415 | 1364 | 16 | 4 | 3 | 1 | βHCH (28) |
| 60 | - | - | 1408 | 1357 | 67 | 15 | 82 | 24 | υCC (24)+βCCC (10) |
| 59 | 1346 | - | 1404 | 1354 | 4 | 1 | 334 | 100 | υCC (10)+βHCC (10)+βHCH (13) |
| 58 | - | - | 1378 | 1328 | 2 | 0 | 3 | 1 | υCC (33)+βHCC (18) |
| 57 | 1302 | 1295 | 1335 | 1287 | 101 | 0 | 4 | 1 | βHCC (34)+τHCCO (22) |
| 56 | 1264 | 1266 | 1308 | 1261 | 131 | 0 | 4 | 1 | βHOC (12)+τHCCO (19) |
| 55 | - | - | 1294 | 1248 | 140 | 0 | 4 | 1 | βHOC (12)+βHCC (31) |
| 54 | - | - | 1277 | 1231 | 31 | 0 | 4 | 1 | υCC (10) |
| 53 | 1227 | - | 1272 | 1226 | 68 | 0 | 8 | 2 | βHOC (17) |
| 52 | - | 1195 | 1246 | 1201 | 49 | 0 | 7 | 2 | υCC (40) |
| 51 | 1175 | 1174 | 1217 | 1173 | 5 | 0 | 10 | 3 | βHCC (17)+τHCOC (30) |
| 50 | - | - | 1199 | 1156 | 10 | 0 | 4 | 1 | υCC (12)+βHCC (11)+τHCOC (23) |
| 49 | - | - | 1190 | 1147 | 1 | 0 | 7 | 2 | βHCC (64) |
| 48 | - | - | 1184 | 1141 | 6 | 0 | 4 | 1 | υOC (12)+υCC (12)+βHCC (21) |
| 47 | - | - | 1169 | 1126 | 1 | 0 | 2 | 1 | βHCH (14)+τHCOC (67) |
| 46 | - | 1121 | 1165 | 1123 | 26 | 0 | 15 | 4 | υCC (30)+βHOC (20) |
| 45 | 1089 | 1092 | 1130 | 1089 | 120 | 0 | 20 | 6 | βCCC (13) |
| 44 | 1071 | 1071 | 1096 | 1057 | 8 | 0 | 1 | 0 | υCC (14) |
| 43 | - | - | 1091 | 1052 | 26 | 0 | 15 | 4 | υCC (32) |
| 42 | 1027 | - | 1083 | 1044 | 13 | 0 | 3 | 1 | υOC (11)+τHCCC (21) |
| 41 | - | 1004 | 1010 | 974 | 0 | 0 | 2 | 1 | υOC (40)+βCCC (25) |
| 40 | - | - | 1007 | 971 | 7 | 0 | 3 | 1 | υCC (22)+τHCCO (10)+τHCCC (14) |
| 39 | 963 | 961 | 994 | 958 | 1 | 0 | 1 | 0 | τHCCC (57) |
| 38 | 923 | - | 973 | 938 | 1 | 0 | 1 | 0 | τHCCC (31) |
| 37 | 894 | 895 | 931 | 897 | 21 | 0 | 2 | 1 | βCCC (27) |
| 36 | - | 865 | 907 | 875 | 10 | 0 | 1 | 0 | βCCC (52)+τCCCC (10) |
| 35 | 859 | - | 866 | 835 | 4 | 0 | 1 | 0 | τHCCC (22) |
| 34 | - | 821 | 854 | 823 | 6 | 0 | 2 | 1 | τHCCC (76) |
| 33 | 819 | - | 845 | 814 | 15 | 0 | 3 | 1 | βCCC (34) |
| 32 | 793 | 793 | 822 | 792 | 12 | 0 | 20 | 6 | τHCCC (21)+ωOCOC (23) |
| 31 | - | - | 804 | 775 | 21 | 0 | 0 | 0 | τCCCC (27) |
| 30 | - | 761 | 780 | 752 | 9 | 0 | 1 | 0 | τHCCC (55) |
| 29 | 741 | 741 | 758 | 731 | 35 | 0 | 0 | 0 | υCC (11) |
| 28 | - | - | 737 | 710 | 9 | 0 | 27 | 8 | βCCC (32) |
| 27 | 672 | - | 696 | 671 | 4 | 0 | 2 | 1 | υOC (12)+βOCO (26) |
| 26 | 641 | 643 | 670 | 646 | 4 | 0 | 1 | 0 | τHCCC (11)+τCCCC (25)+ωCCCC (15) |
| 25 | - | - | 626 | 604 | 7 | 0 | 2 | 1 | βCCC (10)+β OCO (22)+βCOC (10) |
| 24 | 599 | - | 619 | 597 | 3 | 0 | 1 | 0 | βCCC (37)+ωCCCC (18) |
| 23 | 570 | - | 569 | 549 | 26 | 0 | 3 | 1 | τHOCC (74) |
| 22 | - | - | 554 | 534 | 23 | 0 | 4 | 1 | βOCO (13)+βCCC (15) |
| 21 | 527 | 523 | 540 | 521 | 5 | 0 | 1 | 0 | τCCCC (15)+ωCCCC (14) |
| 20 | - | 493 | 519 | 500 | 22 | 0 | 5 | 2 | βHCC (13) |

| | | | | | | | | | |
|---|---|---|---|---|---|---|---|---|---|
| 19 | 483 | - | 505 | 486 | 15 | 0 | 2 | 1 | βCCC (28) |
| 18 | - | - | 483 | 466 | 6 | 0 | 3 | 1 | βCCC (35) |
| 17 | - | - | 465 | 448 | 5 | 0 | 3 | 1 | βOCC (10) |
| 16 | - | 409 | 434 | 419 | 5 | 0 | 1 | 0 | τCCCC (33)+ωCCCC (14) |
| 15 | - | - | 346 | 333 | 1 | 0 | 2 | 1 | βCCC (11)+τOCCC (13) |
| 14 | - | - | 334 | 322 | 0 | 0 | 3 | 1 | βCOC (17)+βCCC (17) |
| 13 | - | 298 | 308 | 297 | 11 | 0 | 7 | 2 | βCCC (14)+βCOC (25) |
| 12 | - | - | 282 | 272 | 0 | 0 | 0 | 0 | τHCOC (17)+τCCCC (43) |
| 11 | - | 231 | 236 | 228 | 1 | 0 | 3 | 1 | βOCC (25)+βCCC (35) |
| 10 | - | - | 229 | 221 | 5 | 0 | 2 | 1 | βOCC (29)+βCOC (17) |
| 9 | - | - | 226 | 218 | 1 | 0 | 1 | 0 | τHCOC (49) |
| 8 | - | 204 | 211 | 203 | 0 | 0 | 0 | 0 | τHCCC (72) |
| 7 | - | 161 | 162 | 156 | 1 | 0 | 1 | 0 | βOCC (23)+βCCC (18)+ωCCCC (21) |
| 6 | - | 146 | 141 | 136 | 3 | 0 | 2 | 1 | τCCCC (30) |
| 5 | - | 117 | 128 | 124 | 0 | 0 | 0 | 0 | βCCC (27)+τ CCCC (13)+ωCCCC (14) |
| 4 | - | 85 | 92 | 89 | 5 | 0 | 1 | 0 | τCOCC (18) |
| 3 | - | - | 48 | 46 | 0 | 0 | 2 | 1 | τCOCC (52)+τCCCC (10) |
| 2 | - | - | 42 | 41 | 6 | 0 | 1 | 0 | τCCCC (37)+τOCCC (19)+τCOCC (11) |
| 1 | - | - | 30 | 29 | 2 | 0 | 4 | 1 | υOC (30)+υCC (15)+βCCC (12) |

Table 2: Observed and calculated vibrational assignments of 3IP2NA.
[a]scaling factor: 0.961 for B3LYP/6-311++G (d,p).
[b]Relative absorption intensities normalized with highest peak absorption equal to 100.
[c]Relative Raman intensities normalized to 100.
υ - Stretching, β - in plane bending, ω - out plane bending, τ - torsion

**O-H vibrations:** The Oxygen- Hydrogen stretching vibrations are expected in the region 3300-3500 $cm^{-1}$. These bands are stronger and broader than those of the aromatic ether O–H stretches which appear in the same region. For the 3IP2NA observed at 3623 $cm^{-1}$ by DFT method. This pure mode shows 100% PED contribution.

**C-H vibrations:** The aromatic compounds and its derivatives show C-H stretching vibrations generally in the region above 3000 $cm^{-1}$ for the benzene and less than 3000 $cm^{-1}$ for non-aromatic compounds [15]. In the experimental frequency, C-H stretching vibrations were observed at 3068 $cm^{-1}$ to 2884 $cm^{-1}$ in FT-Raman spectrum and 3192-2844 in the FT-IR spectra. The peak corresponding to C-H stretching vibration at the range 3079-2901 $cm^{-1}$ by theoretical method shows excellent agreement with experimental spectral values. The PED corresponding to this vibration contributes to 88-98%.

**C-C vibrations:** The aromatic ring modes are influenced more by C-C bands. The ring stretching vibrations (C-C) is expected within the region 1300–1000 $cm^{-1}$ [16-18]. In the present study, the bands which are of different intensities were observed at 1606, 1506, 1484, 1396 and 1348 $cm^{-1}$ in the FT-IR spectrum and Raman bands were identified at 1632, 1582, 1488,1198, and 1004 $cm^{-1}$. The theoretical values were obtained in the range of 1559-999 $cm^{-1}$ by DFT method. It shows that the theoretical values are in good agreement with experimental data.

**O-C Vibrations:** The Oxygen-Carbon stretching modes generally exist in the region 1300-1000 $cm^{-1}$. The theoretical Oxygen-Carbon stretching vibration was calculated at 1724, 1232, 1166, 1100, 1092 and 923 $cm^{-1}$. Experimental bands observed at 1786, 1227, 1175, 1089 and 1071 $cm^{-1}$ in FT-IR and at 1726, 1174, 1121, 1092 and 1071 $cm^{-1}$ in Raman.

## Donor-Acceptor Interactions

In quantum chemistry, a calculated bonding orbital with maximum electron density forms a natural bond orbital (NBO). In computational chemistry, the localized orbital's are used to calculate the distribution of electron

density in atoms and in bonds between atoms. The details obtained about the interactions in both filled and virtual orbital space can complement the study of both inter and intra molecular interactions, which is the basis of studying NBO. That is why NBO analysis is proved to be an important tool for chemical analysis of hyper conjugative interaction and electron density transfer from filled lone electron pairs of the Lewis base (an electron-pair donor) Y into the unfilled anti-bond σ* (X-H) of the Lewis acid (an electron-pair acceptor) X-H in X-Y….Y hydrogen bonding systems [19]. The magnitude of energy of hyper conjugative interactions, E (2) forms the basis of studying the strength of the interaction between electron donors and electron acceptors, or the donating affinity from electron donors to acceptors and hence the degree of conjugation of the entire system. The second-order Fock matrix was done to evaluate the donor-acceptor interactions in NBO analysis [20]. The interactions cause loss of occupancy from the localized natural bond orbitals of the idealized Lewis structure into an empty non-Lewis orbital. For each donor (i) and acceptor (j), the stabilization energy E (2) related to the delocalization, i → j is estimated as

$$E_{(2)} = \Delta E_{ij} = q_i \frac{\left(F(i,j)\right)^2}{\in_j - \in_i}$$

Where $q_i$ is the donor orbital occupancy
$\varepsilon_j$ and $\varepsilon_i$ are diagonal elements
$F_{ij}$ is the off-diagonal NBO Fock matrix element.

Delocalization of electron density between occupied Lewis-type (lone or bond pair) natural bonding orbital's and previously unoccupied non-Lewis (anti-bond or Rydberg) natural bonding orbital's correspond to a stabilizing donor-acceptor interaction. In order to interpret the intermolecular hydrogen bonding, intermolecular charge transfer (ICT) and delocalization of electron density, NBO analysis were performed on the 3IP2NA using B3LYP/6-311++G (d,p) basis set and the corresponding results are presented in (Table 3). The intensity of the interaction between electron donors and electron acceptors is directly dependent on E (2) value, i.e. more the donating tendency from electron donors to electron acceptors, greater is the extent of conjugation of the whole system. The intra-molecular interaction is formed by the orbital overlap between *σ*(C-C) and σ*(C-C) bond orbital which results in intra-molecular charge transfer (ICT) causing stabilization of the system. These interactions are observed as anincrease in electron density (ED) in C-C, C-H, C-O, and O-H anti-bonding orbital that weakens the respective bonds. NBO analysis was performed on the molecule at the DFT/B3LYP6-31++G (d,p) level in order to explicate the delocalization of electron density within the molecule. The delocalization of σ electron from σ (O2-C17) distributes to anti-bonding σ* (C14-H27), σ* (C15-C16), σ* (C15-H29), leading to the stabilization energy of 16.21 kJ/mol, 85.01kJ/mol, 152.83 7 respectively due to conjugative interactions. The intra-molecular hyper conjugative interaction of σ (O2-H31) distribute to σ* (C14-H27), σ* (C15-C16), σ* (C15-H29) leading to stabilization of 212.96 kJ/mol. A strong interaction has been observed due to the electron density transfer from the lone pair LP (1) of oxygen atom (O2) to anti-bonding orbital σ* (C15-H29) with a large stabilization energy of 73.97 kJ/mol. In the case of LP(2) of oxygen atom (O3) to the anti-bonding acceptor σ* (O2-C17) and σ* (C8-C17) has low stabilization energy of 31.17kJ/mol and 14.52 kJ/mol respectively as shown in Table 3. The interaction energy, related to resonance in the molecule, is electron withdrawing from the ring through π* (O3-C17) of the NBO conjugated with π* (C8-C10) resulting with large stabilization energy of 108.51 kJ/mol. Similarly, π (C11-C15) of the NBO conjugated with π* (C15-H29) leading to stabilization energy of 50.96kJ/mol. Therefore, the maximum energy delocalization takes place in the π* – π* transition.

| Donor(i) | Type | ED(e) | Acceptor(j) | Type | ED(e) | E(2)[a] (kJ/mol) | E(j)–E(i)[b] (a.u.) | F(i,j)c (a.u.) |
|---|---|---|---|---|---|---|---|---|
| O2-C17 | σ | | C15-C16 | σ* | 0.01714 | 85.01 | 3.4 | 0.481 |
| O2-C17 | σ | | C15-H29 | σ* | 0.01366 | 152.83 | 3.46 | 0.651 |
| O2-H31 | σ | 1.98776 | C14-H27 | σ* | 0.00553 | 13.83 | 1.02 | 0.106 |
| O2-H31 | σ | | C15-C16 | σ* | 0.01714 | 186.82 | 3.13 | 0.684 |
| O2-H31 | σ | | C15-H29 | σ* | 0.01366 | 212.96 | 3.2 | 0.737 |
| O3-C17 | σ | 1.995 | C14-H27 | σ* | 0.00553 | 12.55 | 1.39 | 0.118 |
| C5-C9 | π | | C8-C10 | π* | 0.31831 | 18.57 | 0.29 | 0.065 |
| C8-C10 | π | 1.69749 | O3-C17 | π* | 0.24118 | 21.2 | 0.27 | 0.069 |
| C8-C10 | π | | C5-C9 | π* | 0.30598 | 23.05 | 0.29 | 0.073 |
| C11-C15 | π | 1.71984 | C14-H27 | σ* | 0.00553 | 40.59 | 1.51 | 0.238 |

| | | | | | | | | |
|---|---|---|---|---|---|---|---|---|
| C11-C15 | π | | C15-C16 | σ* | 0.01714 | 34.65 | 3.63 | 0.34 |
| C11-C15 | π | | C15-H29 | σ* | 0.01366 | 50.96 | 3.69 | 0.416 |
| C11-H21 | σ | 1.98059 | C14-H27 | σ* | 0.00553 | 23.64 | 1.25 | 0.154 |
| C11-H21 | σ | | C15-H29 | σ* | 0.01366 | 20.86 | 3.43 | 0.239 |
| C12-C16 | π | | C11-C15 | π* | 0.26862 | 20.34 | 0.28 | 0.068 |
| O3-C17 | π* | 1.98049 | C8-C10 | π* | 0.31831 | 108.51 | 0.01 | 0.067 |
| O2 | LP(1) | 1.97699 | C15-H29 | σ* | 0.01366 | 73.97 | 3.17 | 0.433 |
| O2 | LP(2) | 1.97699 | O3-C17 | π* | 0.24118 | 40.52 | 0.35 | 0.108 |
| O3 | LP(2) | 1.98049 | O2-C17 | σ* | 0.30598 | 31.17 | 0.59 | 0.122 |
| O3 | LP(2) | 1.98049 | C8-C17 | σ* | 0.05816 | 14.52 | 0.71 | 0.093 |

Table 3: Second order perturbation theory analysis of Fock matrix in NBO basis of 3IP2NA.
[a]E(2) means energy of hyper conjugative interaction (stabilization energy)
[b]E(j) – E(i) is the energy difference between donor i and acceptor j
[c]F(i,j) is the Fock matrix element between i and j NBO orbital's

## HOMO and LUMO Analysis

The concept of HOMO and LUMO are of fundamental importance as it forms the basis of understating the chemical stability and reactivity of a given molecule. On the basis of chemical hardness, molecules can be classified as hard and soft molecules. Large HOMO-LUMO gap indicates that the title molecule is a hard molecule and minor HOMO-LUMO gap indicates that it is a soft molecule. The molecular stability and hardness are related inversely, i.e. the molecule with the least HOMO-LUMO gap is more reactive. The ionization potential (IP) is determined from the energy difference between the energy of the compound derived from electron- transfer ($E_{cation}$ - energy of radical cation) and the respective neutral compound ($E_n$)

$$IP = E_{cation} - E_{n;}\ IP = -E_{HOMO.}$$

The electron affinity (EA) is computed from the energy difference between the neutral molecule ($E_n$) and the anion molecule ($E_{anion}$)

$$EA = E_n - E_{anion};\ EA = -E_{LOMO.}$$

The minimum energy required to promote an electron is given by the energy difference between the orbitals (energy gap) and is therefore, the most frequent and important energy transfer mechanism within a system. The orbitals provideinformation about the electron density which in turn is used in determining which part of the molecule is most actively participating in an energy transfer event.

The calculated quantum chemical parameters such as the highest occupied molecular orbital energy ($E_{HOMO}$), the lowest unoccupied molecular orbital energy ($E_{LUMO}$), energy gap (ΔE), Electro negativity (χ), chemical potential (μ), global hardness (η) and the softness (S) were calculated for the 3IP2NA and tabulated in (Table 4). The concept of these parameters is related to each other [21-25], where

Chemical potential ($\mu$) = ½ ($E_{LUMO}$ +$E_{HOMO}$),
Electro negativity ($\chi$) = $-\mu$ = - ½ ($E_{LUMO}$ +$E_{HOMO}$),
Global hardness ($\eta$) = ½ ($E_{LUMO}$ - $E_{HOMO}$),
Electro philicity (ω) = $\mu^2$ / 2$\eta$.

The inverse values of the global hardness are designated as the softness(S), it is given by Softness ($S$) = 1/$\eta$

The calculated value of electrophilicity index = 3.7165 describes the biological activity of 3IP2NA. Also the bigger the dipole moment, the stronger will be the intermolecular interactions. Correlations have been deduced between electrophilicity of several chemical compounds and reaction rates in biochemical systems and such phenomena as allergic contact dermatitis. The energy of the HOMO and the ionization potential are related and describes the susceptibility of the molecule toward electro philic attack. The energy of LUMO is directly linked to the electron affinity [26] and illustrates the susceptibility of the molecule toward attack of nucleophiles. The energy gap between HOMO and LUMO indicates molecular chemical stability. The mesh diagrams of HOMO and LUMO are given in Figure 3. The positive and negative phase is represented in red and blue colour respectively.

| Parameter | Value |
|---|---|
| $E_{HOMO}$ (eV) | -6.0309 |
| $E_{LUMO}$ (eV) | -1.8515 |
| Ionization potential | 6.0309 |
| Electron affinity | 1.8515 |
| Energy gap (eV) | 4.1794 |
| Electro negativity | 3.9412 |
| Chemical potential | -3.9412 |
| Chemical hardness | 2.0897 |
| Chemical softness | 0.2393 |
| Electrophilicity index | 3.7165 |

Table 4: Calculated energy values of 3IP2NAby B3LYP/6-311++G (d,p).

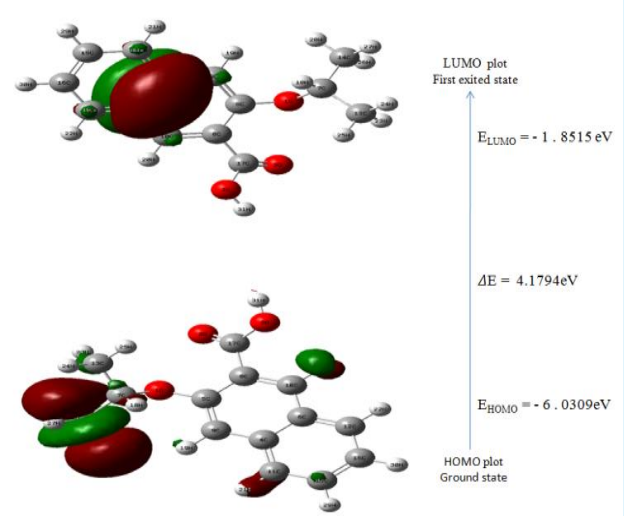


Figure 3: HOMO - LUMO plots of 3IP2NA.

charges. Molecular electrostatic potential maps elucidate information about the charge distribution of a molecule, relative polarity, and electrostatic potential properties of the nucleus and nature of electrostatic potential energy.

MEP is associated with the electronic density and is an expedient descriptor in understanding sites for electrophilic and nucleophilic reactions as well as hydrogen bonding interactions. MEP was calculated at the B3LYP/6-311++G (d,p) optimized geometry. In MEP, the maximum negative region represents the site for electrophilic attack indicated by red color while the maximum positive region represents nucleophilic attack indicated in blue color. While regions with the negative potential are over the electronegative oxygen atom, the regions with the positive potential are over the hydrogen atoms. Potential increases in the order red < orange < yellow < green < blue. Figure 4 provides a visual method to understand the relative polarity of the 3IPN2A.

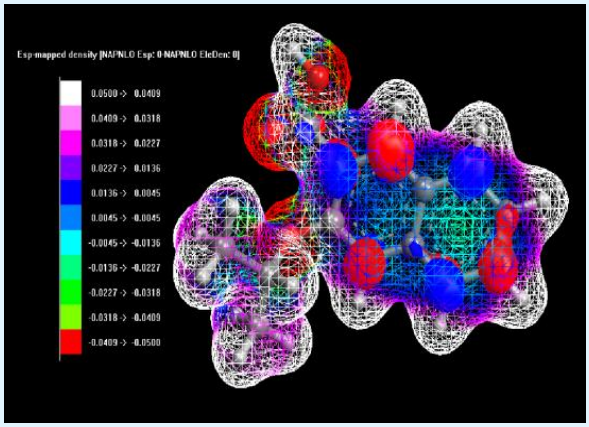

Figure 4: MEP on 3IPN2A.

## Molecular Electrostatic Potential (MEP)

The force acting on a proton located at a point through the electrical charge cloud generated through the molecules electrons and nuclei provides the MEP at a given point p(x,y,z) in the vicinity of a molecule [27,28]. Although the molecular charge distribution remains unperturbed through the external test charge as no polarization occurs, the electrostatic potential of a molecule is a good tool in evaluating the reactivity of a molecule towards positively or negatively charged reactants. The MEP is characteristically pictured through mapping its values onto the surface reflecting the molecules boundaries. Electrostatic potential correlates with a dipole moment, electronegativity and partial

## Thermodynamic Properties

The partition function is one of the important parameters of thermodynamics. The partition function associates thermodynamics, spectroscopy and quantum theory. The standard statistical thermodynamic functions such as standard heat capacity ($C_P$), standard entropy (S), and standard enthalpy changes (H) were obtained from the theoretical harmonic frequencies on the basis of vibrational analysis at B3LYP/6-311++G (d,p) level using Thermo.pl software and listed in Table 5. From the observations in the above (Table 6), all the values of $C_p$, S, and H increases with the increase in temperature from 100 K to 1000 K. This is accredited to the enhancement of the molecular vibration. The temperature increases

because at a constant pressure, the values of Cp, S and H are equal to the quantity of temperature [29]. The relations between these thermo dynamic properties and temperatures are fitted by quadratic equations and the corresponding fitting factor ($R^2$). It was found to be 0.99999, 0.99934 and 0.99938 for entropy, heat capacity, and enthalpy, respectively. The temperature dependence correlation graphs are represented in (Figure 5) and the corresponding fitting equations are shown below [30]

$S = 244.9274 + 0.9992T - 2.15526\times10^{-4}T^2$ ($R^2 = 0.99999$).

$C_P = 8.63323 + 0.95984T - 3.9441\times10^{-4}T^2$ ($R^2 = 0.99934$).

$H = -10.55911 + 0.01479T + 2.64559\times10^{-4}T^2$ ($R^2 = 0.99938$)

Thermodynamic energies according to the relationships of thermodynamic functions can be calculated and estimated directions of chemical reactions in agreement with the second law of thermodynamics in the thermo chemical field can be evaluated [31].

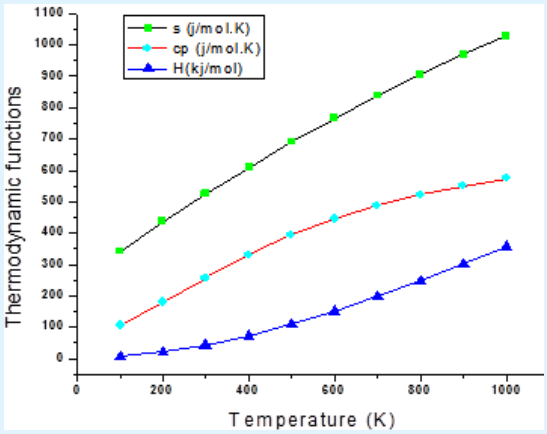


Figure 5: Correlation graphic of heat capacity, entropy, enthalpy at different temperature for 3IPN2A

| Temperature(K) | S°m (cal.mol-1K-1) | $C^o_{pm}$ ( cal.mol-1K-1) | ΔH°m (kcal.mol-1) |
|---|---|---|---|
| 100 | 341.76 | 106.616 | 6.927 |
| 200 | 437.878 | 179.826 | 21.212 |
| 298.15 | 523.793 | 255.859 | 42.58 |
| 300 | 525.38 | 257.291 | 43.055 |
| 400 | 609.712 | 331.137 | 72.546 |
| 500 | 690.61 | 394.28 | 108.917 |
| 600 | 767.216 | 445.822 | 151.013 |
| 700 | 839.194 | 487.71 | 197.76 |
| 800 | 906.639 | 522.149 | 248.307 |
| 900 | 969.846 | 550.855 | 301.999 |
| 1000 | 1029.172 | 575.05 | 358.328 |

Table 5: Thermodynamics functions of 3IPN2A with different temperature.

## Mulliken Population Analysis

The natural population analysis of 3IP2NA obtained by Mulliken [32,33] population analysis using B3LYP/ 6-311++G (d,p) method. Mulliken atomic charge calculation has an important role for the application of quantum chemical calculation of the molecular system. Atomic charge affects dipole moment, polarizability, electronic structure and other molecular properties of the system. The calculated Mulliken charge values of 3IP2NA are listed in Table 6. It can be observed graphically in Figure 6 that the carbon atom (C17) has more negative charge whereas all the hydrogen atoms have the positive charges. The positive charge of carbon is found C1, C2, C5, C11 and C15 in our compound. Carbon 17 has more positive charge compared to other atoms. The carbon atom is identified positive and negative charges. The carbon negative charge is identified C17 and positive is identified at C1, C2, C5, C11 and C15. The oxygen atom is clearly shown negative charge and all the hydrogen atoms have positive charges. Similarly, themore negative charge is also carried by the carbon atom (C17) and less positive charge of carbon atom was identified at C1, C2, C5, C11, and C15 due to carbonyl, ether oxygen group and dimethyl groups. One oxygen atom has a negative charge and all the hydrogen atoms have positive charges. The result suggests that the oxygen atom acted as lone paired donor.

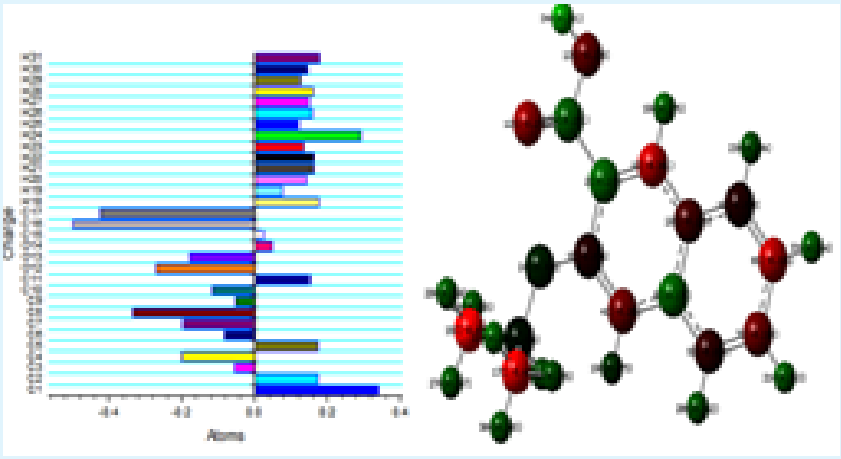

Figure 6: Illustration of Mulliken atomic charges of 3IP2NA.

| Atom | Charge | Atom | Charge |
|---|---|---|---|
| C1 | 0.34080 | C17 | -0.42280 |
| C2 | 0.17461 | H18 | 0.17603 |
| C3 | -0.05373 | H19 | 0.07469 |
| C4 | -0.20075 | H20 | 0.14169 |
| C5 | 0.17295 | H21 | 0.16296 |
| C6 | -0.08286 | H22 | 0.16351 |
| C7 | -0.19837 | H23 | 0.13377 |
| C8 | -0.33473 | H24 | 0.29056 |
| C9 | -0.05322 | H25 | 0.12185 |
| C10 | -0.11635 | H26 | 0.15629 |
| C11 | 0.15123 | H27 | 0.14732 |
| O12 | -0.26960 | H28 | 0.16005 |
| O13 | -0.17802 | H29 | 0.12615 |
| O14 | 0.04787 | H30 | 0.14569 |
| C15 | 0.02385 | H31 | 0.17935 |
| C16 | -0.49917 | | |

Table 6: Mulliken atomic charges of 3IP2NA.

## Molecular Modeling Analysis

Auto Dock- automated docking software designed to predict how small molecules (substrates or drug candidates) bind to a receptor of the known 3D structure. The 3IP2NA was selected to be docked into the active site of the proteins 4XUV and 4M1C were obtained from (www.rcsb.org) protein data bank. The ligand was docked into the functional sites of the relevant proteins independently and the docking energy was a check to achieve a minimum value. Auto Dock results indicate the binding position and bound conformation of the peptide, together with a bumpy estimate of its interaction. Docked conformation which had the minimum binding energy was preferred to figure out the mode of binding. Auto Dock binding energies (kcal/mol) and inhibition constants (μm) were also obtained and publicized in Table 7. Among them, 4XUV exhibited the lowest free energy at −5.40 kcal/mol and most docked inhibitors interacted with the ligand within the 4XUV binding site. They exhibited up to four hydrogen bonds involving SER 292, MET 359, SER 358 and SER 358 with RMSD being 50.74 Å. The 3IP2NA ligand interacts with different receptors are shown in Figures 7 a & b.

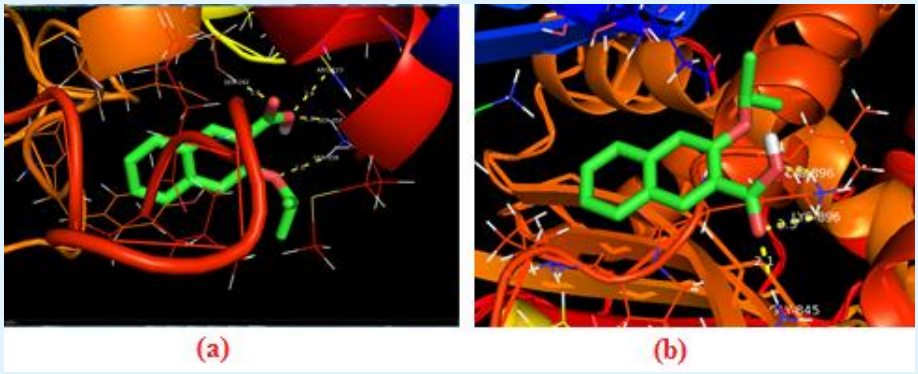


Figure 7: Docking and Hydrogen bond interactions of 3IP2NA with (a) 4XUV and (b) 4MIC.

| Protein (PDB ID) | Bonded residues | Bond distance (Å) | No. of hydrogen bond | Binding energy (kcal/mol) | Estimated Inhibition Constant (µm) | Reference RMSD (Å) |
|---|---|---|---|---|---|---|
| 4XUV | SER292 | 1.8 | 4 | -5.4 | 110.43 | 50.74 |
| | MET359 | 2.8 | | | | |
| | SER358 | 1.8 | | | | |
| | SER358 | 2.5 | | | | |
| 4M1C | LYS566 | 2.1 | 3 | -4.99 | 221.5 | 78.02 |
| | LYS896 | 2.5 | | | | |
| | LYS896 | 2.2 | | | | |

Table 7: Hydrogen bonding and molecular docking with 4XUV and 4M1C.

## Conclusion

In the present work, the optimized molecular structure, electronic properties, vibrational frequencies and the intensity of vibrations of the 3IP2NAare calculated by DFT method using B3LYP/6-311++G (d,p) basis set. The optimized geometric parameters are theoretically determined by DFT theory. The vibrational FT-IR and FT-Raman spectra of the ADHPT molecule are recorded and on the basis of agreement between the calculated and experimental results, the assignments of all the fundamental vibrational modes of the 3IP2NAare made unambiguously based on the results of the PED. The possible electrophilic and nucleophilic reactive sites of the molecule were predicted and the intra molecular interactions of the molecule were also confirmed through NBO analysis. Low HOMO–LUMO energy gap value indicates the intra molecular charge transfer takes place within the molecule. The charge and multiplicity are varied in order to compare the variation in the Mullikan charges in each case. Fukui function helps to identify the electrophilic / nucleophilic nature of a specific site within a molecule. The MEP shows the negative potential sites are on oxygen atoms as well as the positive potential sites around the hydrogen atoms. Molecular docking of the title compound is also reported due to the different biological activity of 3IP2NA.

## References

1. Szafran M, Komasa A, Admska EB (2007) Crystal and molecular structure of 4-carboxypiperidinium chloride (4-piperidinecarboxylic acid hydrochloride). Journal of Molecular Structure 827(1): 101-107.

2. James C, Amal A, Reghunathan R, Hubert JI, Jayakumar VS (2006) Structural conformation and vibrational spectroscopic studies of 2,6-bis (p-N,N-dimethyl benzylidene) cyclohexanone using density functional theory. J Raman Spectrosc 37(12): 1381-1392.

3. Lu JN, Chen ZR, Yuan SF, Zhejiandg (2005) J Univ Sci B 6: 584-589.

4. Shoba D, Periandi S, Boomadevi S, Ramalingam S, Fereyduni E (2014) FT-IR, FT-Raman UV, NMR spectra, molecular structure, ESP, NBO and HOMO–LUMO investigation of 2-methylpyridine 1-oxide: A combined experimental and DFT study. Spectrochim Acta 118: 438-447.

5. Salathé M, Kazandjieva M, Lee JW, Levis P, Feldman MW, et al. (2010) A high-resolution human contact network for infectious disease transmission. Proc Natl Acad Sci U S A 107(51): 22020-22025.

6. Rawal RK, Prabhakar YS, Katti SB, De Clercq E (2005) 2-(Aryl)-3-furan-2-ylmethyl-thiazolidin-4-ones as selective HIV-RT inhibitors DeClercq. Bioorg Med Chem 13(24): 6771-6776.

7. Bonde CG, Gaikwad NJ (2004) Synthesis and preliminary evaluation of some pyrazine containing thiazolines and thiazolidinones as antimicrobial agents. Bioorg Med Chem 12(9): 2151-2161.

8. Frisch MJ (2009) Gaussian 09, Gaussian Inc, Wallingford, CT, USA.

9. Dennington R, Keith T, Millam J (2007) Gauss View, Version 4.1.2, Semichem Inc. Shawnee mission, KS.

10. Jamroz MH, Vibrational Energy Distribution Analysis VEDA 4, Warsaw, 2004-2010.

11. Morris GM, Huey R, Lindstrom W, Sanner MF, Belew RK, et al. (2009) Auto Dock 4 and Auto DockTools4: automated docking with selective receptor flexibility. J Comput Chem 30 (16): 2785- 2791.

12. Keresztury G (2002) Raman spectroscopy: Theory in Handbook of vibrational spectroscopy.

13. Muthu S, Ramachandran G, Isac Paulraj E, Swaminathan T (2014) Quantum mechanical study of the structure and spectroscopic (FTIR, FT-Raman), first-order hyperpolarizability and NBO analysis of 1,2-benzoxazol-3-ylmenthane sulfonamide. Spectrochim Acta A 128(15): 603-613.

14. Vetrivelan V (2018) Spectra, Electronic Properties, Biological Activities and Molecular Docking Investigation on Sulfonamide Derivative Compound: An Experimental and Computational Approach. J Nanosci Tech 4(2): 348-352.

15. Stetter H, Rauscher E (1960) Über Verbindungen mit Urotropin-Struktur, XIX. Zur Kenntnis des β-[Adamantyl-(1)]-β-oxo-propionsäure-äthylesters. Chem Ber 93(9): 2054-2057.

16. Karabacak M, Karaca C, Atac A, Eskici M, Karanfil A (2012) Synthesis, analysis of spectroscopic and nonlinear optical properties of the novel compound: (S)-N-benzyl-1-phenyl-5-(thiophen-3-yl)-4-pentyn-2-amine. Spectrochim Acta A 97: 556-567.

17. Surisseau C, Marvell P, Raman J (1994) Spect 25: 447-455.

18. Barnes AJ, Majid MA, Stuckey MA, Gregory P, Stead C (1985) The resonance Raman spectra of Orange II and Para Red: molecular structure and vibrational assignment. Spectrochim Acta A 41(4): 629-635.

19. Weinhold F, Landis CR (2005) Valency and Bonding: A Natural Bond Orbital Donor-Acceptor Perspective, Cambridge University Press, Cambridge.

20. Sidir I, Sidir YG, Kumalar M, Tasal E (2010) Ab initio Hartree–Fock and density functional theory investigations on the conformational stability, molecular structure and vibrational spectra of 7-acetoxy-6-(2,3-dibromopropyl)-4,8-dimethylcoumarin molecule. J Mol Struct 964(1-3): 134-151.

21. Parr RG, Szentpaly L, Liu S (1999) Electrophilicity Index. J Am Chem Soc 121 (9): 1922-1924.

22. Chattraj P, Maiti B, Sarkar U (2003) J Phys Chem 107 (25): 4973-4975.

23. Parr RG, Donnelly R, Levy M, Palke W (1978) Electronegativity: The density functional viewpoint. J Chem Phys 68(8): 3801-3807.

24. Parr RG, Pearson R (1983) Absolute hardness: companion parameter to absolute electro negativity. J Am Chem Soc 105 (26): 7512-7516.

25. Parr RG, Chattraj P (1991) Principle of maximum hardness. J Am Chem Soc 113(5): 1854-1855.

26. Gunasekaran S, Balaji RA, Kumeresan S, Anand G, Srinivasan S (2008) Experimental and theoretical investigations of spectroscopic properties of N-acetyl-5-methoxytryptamine. Can J Anal Sci Spectrosc 53: 149-155.

27. Sebastin S, Sundaraganesan N (2010) The spectroscopic (FT-IR, FT-IR gas phase, FT-Raman and

UV) and NBO analysis of 4-Hydroxypiperidine by density functional method. Spectrochim Acta A 75(3): 941-952.

28. Luque EJ, Lopez JM, Orozco M (2000) Perspective on "Electrostatic interactions of a solute with a continuum. A direct utilization of ab initio molecular potentials for the prevision of solvent effects. Theor Chem Acc 103(3-4): 343-350.

29. Bopp F, Meixner J, Kestin J (1967) Thermodynamics and Statistical Mechanics, 5th (ed), Press Inc Ltd, London, New York.

30. Bhavani K, Renuga S, Muthu S, Sankaranarayanan K, Spectrochim Acta A, Mol and Bio mol Spectroscopy, 136: 1260-1268.

31. Zhang R, Dub B, Sun G, Sun Y (2010) Experimental and theoretical studies on o-, m- and p-chlorobenzylidene amino antipyrines. Spectrochim Acta A 75(3): 1115-1124.

32. Mulliken RS (1995) Electronic Population Analysis on LCAO–MO Molecular Wave Functions I. J Chem Phys 23(10): 1833-1840.

33. Sidir I, Sidir YG, Kumalar M, Tasal E (2010) Ab initio Hartree-Fock and density functional theory investigations on the conformational stability, molecular structure and vibrational spectra of 7-acetoxy-6-(2,3-dibromopropyl)-4,8-dimethylcoumarin molecule. J Mol Struct 964(1): 134-151.